Structure determination and a vibrational study for the hexagonal elpasolite $Cs_2NaGaF_6:Cr^{3+}$

2002 J. Phys.: Condens. Matter 14 12383

(http://iopscience.iop.org/0953-8984/14/47/312)

INSTITUTE OF PHYSICS PUBLISHING JOURNAL OF PHYSICS: CONDENSED MATTER

J. Phys.: Condens. Matter **14** (2002) 12383–12389 PII: S0953-8984(02)37388-0

Structure determination and a vibrational study for the hexagonal elpasolite Cs_2NaGaF_6:Cr^{3+}

H N Bordallo[1,2], X Wang[1], K M Hanif[3], G F Strouse[3], R J M da Fonseca[4], L P Sosman[4] and A Dias Tavares Jr[4]

[1] Intense Pulsed Neutron Source, Argonne National Laboratory, Argonne, IL 60439, USA
[2] Hahn-Meitner-Institut-Berlin, SF-1 Gleinicker Straße, 100 D-14109, Berlin, Germany
[3] Department of Chemistry, UC Santa Barbara, Santa Barbara, CA 93106, USA
[4] Instítuto de Física, UERJ, Rua São Francisco Xavier, 524, Rio de Janeiro, 20550, Brazil

E-mail: bordallo@hmi.de

Received 23 May 2002
Published 15 November 2002
Online at stacks.iop.org/JPhysCM/14/12383

Abstract

Single crystals of 0.5% Cr^{3+}-doped Cs_2NaGaF_6 were studied by means of x-ray diffraction and polarized Raman scattering. The crystal exhibits a unique stacking interaction, with a hexagonal structure with $R\bar{3}m$ symmetry. Polarized Raman spectra recorded at 16 and 300 K reveal sidebands that are ascribed to the local vibrational of the $[CrF_6]$ coordination unit, which differ markedly from those of the Cs_2NaGaF_6 host lattice. The results are compared to findings for other elpasolite lattices, and the room temperature luminescence quantum yields are discussed in terms of a delicate balance between electron–phonon strength and lattice distortion.

1. Introduction

Numerous studies have been dedicated to the optical properties of Cr^{3+} as an impurity ion in an extended lattice [1], and more particularly in the development of solid-state lasers. The most prominent example is that of ruby, i.e. Cr^{3+} in Al_2O_3, where extensive studies of the optical properties led to the development of the first laser ever operated [2]. In the research on broadband lasers, particular attention has been focused on Cr^{3+}-doped crystalline hosts [3–7]. In this context, Cr-doped elpasolite provides an excellent model system in which to investigate crystal-field and vibronic coupling effects. In this system the electron–phonon (el–ph) interaction between the impurity centre and the host lattice is weaker than in oxide hosts, and a broad band dominates the emission spectrum. This is a fundamental property for tunable laser applications, given that the broader the emission band, the larger the tuning range.

Recently [7], we observed at 300 K a broad vibronic band that extends from the visible to the near-infrared spectral region in Cs_2NaMF_6:Cr^{3+} (M = Ga and Al) emission spectra. As

these compounds lie near the boundary between low-field and high-field chromium complexes, the Cr^{3+} $^4T_2 \rightarrow {}^4A_2$ spin-allowed transition dominates the fluorescence spectrum at room temperature, while at 77 and 4.2 K the fluorescence originates from the $^2E \rightarrow {}^4A_2$ transition. Moreover the competition between the distortions in the t_{2g}, e_g, and a_{1g} coordinates will favour radiative emission at room temperature and account for a reasonable quantum yield (η) observed in the Cr^{3+}-doped fluorides.

To better understand the origin of the broadness of the emission line in these systems, it is important to understand the trend followed by the M^{3+}–F distances, due to the differences between the ionic radii, r_{Ga} (0.62 Å) > r_{Cr} (0.615Å) > r_{Al} (0.53 Å), as well as the el–ph coupling strength. With this in mind, we carried out a systematic study of several Cr^{3+}-doped elpasolite lattices. Here we report on single-crystal x-ray and Raman spectroscopy (RS) measurements for 0.5% Cr^+-doped Cs_2NaGaF_6. A comparison to previous work [8] allows us to obtain a correlation of the nonradiative quenching with the size of the unit cell and with the extent of the el–ph interaction in the Cs_2NaMF_6 system.

2. Experimental details

As previously described [7], single-crystal samples with 0.5% Cr^{3+} doping were prepared by hydrothermal methods at the Institute of General and Inorganic Chemistry in Moscow.

X-ray diffraction experiments were performed at room temperature on a Siemens SMART CCD area detector diffractometer. Refinements of the single-crystal structure, after applying extinction corrections, were performed using as a starting model the elpasolite structure [8] of Cs_2NaMF_6:Cr^{3+}. Also it was assumed that for a fixed Cr/Ga ratio the Cr would randomly replace some of the Ga atoms. This model was refined using the Shelx-97 package to an *R*-value of 0.018.

Polarized, single-crystal Raman scattering measurements were collected in a back-scattering configuration on a 0.5 M ARC single spectrograph (1800 lines mm^{-1}/400 blaze) coupled to a Princeton Instruments LN2 512 × 512 CCD array. Laser light rejection was accomplished by a Notch filter (Kaiser optical) before the entrance slit. Excitation (488.0 nm, 3.0 mW) was provided by a 10 W Spectra-Physics 2200 Ar^+-ion laser. A 5 nm band pass was used to suppress the plasma lines. Polarization measurements were carried out by laser polarization rotation at a $\lambda/4$ plate and collection of the scattered Raman intensity through a calcite polarizer. All scattering data were collected through a depolarizer prior to coupling into the spectrograph to eliminate instrumental polarization dependences. Wavenumber calibrations were carried out using argon lamps. Temperature control at ±1.0 K was provided by an APD Heli-Tran cryostat controlled by a SI 9620-1 temperature controller.

3. Results

3.1. Crystal structure determination

Table 1 presents the collection parameters for the x-ray diffraction data for Cs_2NaGaF_6:0.5% Cr^{3+}. The crystal shows a hexagonal structure with $R\bar{3}m$ (D^5_{3d}) symmetry, with a framework composed of GaF_6 octahedra that are interconnected through face-and corner-sharing NaF_6 octahedra. As shown in figure 1, the structure is designated as '12 L-type', because twelve layers of Ga and Na polyhedra stack along the *c*-axis. The atomic positions and isotropic equivalent thermal parameters are given in table 2. Due to its low concentration, the Cr occupancy in the Ga sites could not be determined within experimental error. However, considering that the most important factors for substitution are the ionic radius ($r_{Ga^{3+}} = 0.62$ Å,

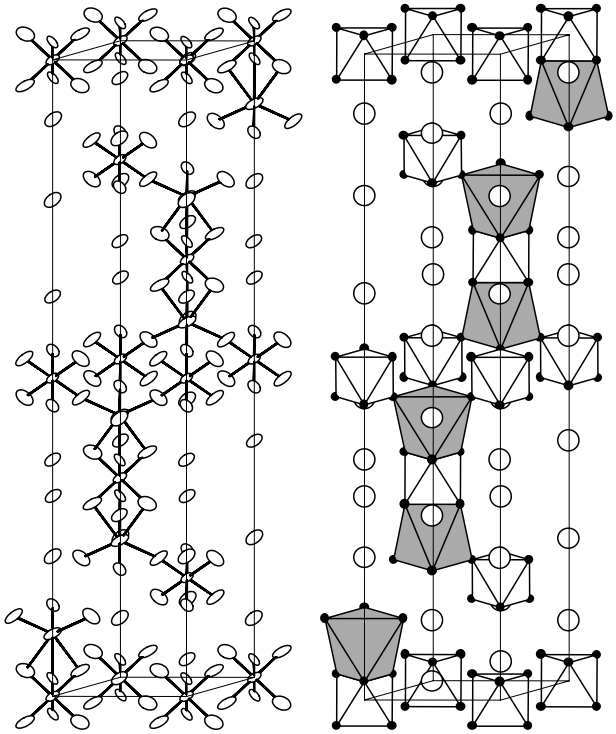

Figure 1. An Ortep view (left) and a polyhedral representation (right) from the neutron refinement showing the connectivity between the GaF_6 and the NaF_6 octahedra. The white and grey polyhedra represent GaF_6 and NaF_6, respectively, while the white and black atoms correspond to Ce and F. The ellipsoid probabilities were drawn at 90%. Some of the octahedra were removed for clarity.

Table 1. X-ray data collection parameters for $Cs_2NaGaF_6:Cr^{3+}$.

Temperature (°C)	23
Crystal size (mm)	$0.5 \times 0.25 \times 0.25$
Space group	$R\bar{3}m$ (No 166)
a (Å)	6.244(1)
c (Å)	30.270(4)
V (Å^3)	1022.1(2)
Z	6
Radiation	X-ray, $\lambda = 0.710\,73$ Å
Data collection technique	Siemens Smart CCD
Extinction parameter	0.005 57
No of reflections before averaging	3553
No of unique reflections	357
Variables	28
Function minimized	$\sum w(F_0 - F_c)^2$
Refinement type	F^2
$R_w(F^2)/wR2$	0.0434
$R(F)/R1$	0.0183
GOF	1.147

Table 2. Atomic positions and isotropic equivalent thermal parameters for $Cs_2NaGaF_6:Cr^{3+}$.

Site symmetry	Atom	x	y	z	U_{eq}
$3a(m)$–D_{3d}	Ga(1)	0.0	0.0	0.0	1.13
$3b(m)$–D_{3d}	Ga(2)	0.0	0.0	0.5	0.93
$6c(3m)$–C_{3v}	Na	0.0	0.0	0.097 68(10)	1.59
$18h(.m)$–C_s	F(1)	0.1408(2)	−0.1408(2)	0.962 39(8)	1.70
$18h(.m)$–C_s	F(2)	0.1888(2)	−0.1888(2)	0.130 85(8)	1.99
$6c(3m)$–C_{3v}	Cs(1)	0.0	0.0	0.780 875(16)	1.81
$6c(3m)$–$C3_{3v}$	Cs(2)	0.0	0.0	0.628 079(15)	1.62

Table 3. Interatomic distances for the isostructural Cs_2NaMF_6 elpasolites, for M = Al, Ga, Cr, and Fe.

Interatomic distance (Å)	$Cs_2NaAlF_6:0.5Cr^{3+}$ [a]	$Cs_2NaGaF_6:0.5Cr^{3+}$ [b]	Cs_2NaCrF_6 [c]	Cs_2NaFeF_6 [c]
M(1)–F(1)	1.813(5)	1.902(2)	1.906(5)	1.930(4)
M(2)–F(2)	1.820(5)	1.901(2)	1.913(6)	1.922(4)
Na–F(1)	2.361(1)	2.371(3)	2.370(6)	2.377(6)
Na–F(2)	2.2958(5)	2.275(3)	2.272(7)	2.266(6)

[a] Reference [8].
[b] This work.
[c] Reference [9]

$r_{Cr^{3+}} = 0.615$ Å, and $r_{Na^+} = 0.97$ Å) and the valence (as for the Ga and Cr ions), we can argue that the Cr^{3+} ions enter into the host substitutionally replacing the Ga^{3+} ions, and not the Na^+. Furthermore, on the basis of previous optical spectra studies on $Cs_2NaGaF_6:Cr^{3+}$ [7], we know that the Cr^{3+} ions occupy octahedral sites, and are not randomly distributed in the lattice.

In Cs_2NaGaF_6, as in other hexagonal elpasolites [9–11] of $R\bar{3}m$ (D^5_{3d}) symmetry, there are two crystallographically distinct Ga positions, Ga(1) and Ga(2), which are at high-symmetry positions. The regular fluoride octahedra around the central Ga(1) ion share two trigonal faces with Na polyhedra along the c-axis (site 1), while the Ga(2) octahedra share all six corners with six different Na polyhedra (site 2). On the other hand, the sodium fluoride polyhedron (NaF_6) is distorted, with unequal Na–F(1) and Na–F(2) distances, and the Cs atoms sit in large cavities formed by twelve fluoride atoms.

As shown in table 3, the measured bond distances in $Cs_2NaGaF_6:Cr^{3+}$ are comparable to those observed in similar structures [8, 9]. A closer inspection of the M–F interatomic distances reveals that the introduction of Cr^{3+} in the Cs_2NaMF_6 (M = Al, Ga) host lattice causes a bigger M^{3+}–F bond-length variation in the aluminate system. This result is in perfect agreement with previous time-resolved emission results [7], which also indicated that the sites occupied by the Cr^{3+} ions are more distorted in the doped Cs_2NaAlF_6. This larger distortion can be understood in terms of the difference in ionic radius (r): given that the values of $r_{Ga^{3+}}$ and $r_{Cr^{3+}}$ are very close, $r_{Ga^{3+}}$ (0.62 Å) > $r_{Cr^{3+}}$ (0.615 Å) > $r_{Al^{3+}}$ (0.53 Å), it is easier to accommodate the Cr^{3+} ion in the Cs_2NaGaF_6 lattice than in Cs_2NaAlF_6.

3.2. Identification of the Raman-active modes

From a group theoretical analysis of the primitive cell [8], the phonons in $Cs_2NaAlF_6:0.5Cr^{3+}$ can be classified as $7A_{1g} + 2A_{1u} + 9A_{2u} + 2A_{2g} + 9E_g + 11E_u$, where only the A_{1g} (xx, yy, zz) and E_g (xy, xz, yz) modes are Raman active.

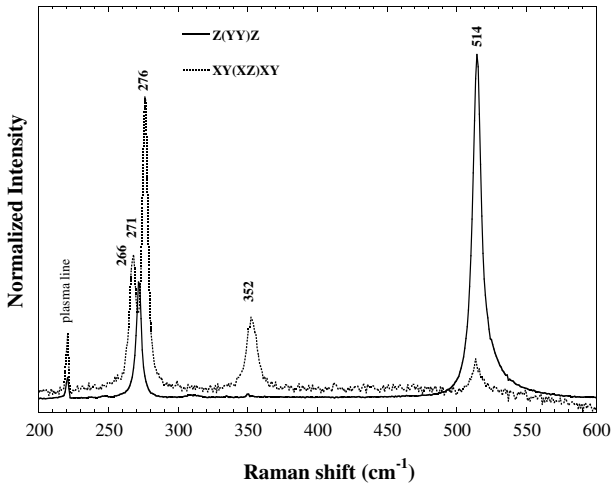

Figure 2. Polarized room temperature Raman spectra of Cs_2NaGaF_6:Cr^{3+} (0.5%) for different sample orientations. The Raman modes (A_{1g} at 271 and 514 cm^{-1} and E_g at 266, 276, and 352 cm^{-1}), as well as a plasma line observed at 220 cm^{-1}, are labelled in the figure. As the intensity of the $XY(XZ)XY$ spectra is three times lower than that of the $Z(YY)Z$ ones, the data were normalized.

Room temperature Raman spectra are shown in figures 2(a) and (b). The measurements were performed in two different scattering geometries $Z(YY)Z$ and $XY(XZ)XY$, allowing the observed Raman modes to be unambiguously determined. Polarization rules impose that for the $Z(YY)Z$ configuration, mainly the modes of A_{1g} (zz) symmetry should be observed, while in orientation 2, $XY(XZ)XY$, light is predominantly scattered by the E_g (xz) mode.

Of the sixteen Raman-active modes, only five modes (two A_{1g}s and three E_gs) are observed between 200 and 600 cm^{-1}. The Cs-ion lattice mode is expected to be observed at lower frequencies (<80 cm^{-1}) [12] while the mode for the Ga ion is IR active, and not observed in the Raman data. Considering that the intensity of Raman modes in an XY_6 molecule normally follows the order $I(A_{1g}) > I(E_g)$ [13], and by comparison with previous results [8, 14, 15], the observed modes were assigned. The A_{1g} modes at 271 and 514 cm^{-1} arise predominantly from F-ion stretching modes in the D_{3d} factor group for the crystal. The modes at 266, 276, and 352 cm^{-1} can be assigned to E_g modes corresponding to motions of the Na and F ions in the xy-plane based on the polarization data.

The sidebands of the modes located at 278 and 530 cm^{-1}, whose resolution is enhanced on cooling (see figure 3), are attributed to $[CrF_6]^{3-}$ normal modes. These values agree with the frequencies found in the literature for such complexes in different crystals [16], and also with well-defined vibrational structure observed in Cs_2NaGaF_6:0.5% Cr^{3+} luminescence spectra [7]. Since the mode located at 530 cm^{-1} lies at a frequency higher than the frequency cut-off of the system, it can be attributed to a true localized mode.

4. Discussion and conclusions

The crystal structure for elpasolites A_2BMF_6 depends on the radius ratio of the ions in the lattice, as described by the Goldschmidt tolerance factor [8] (t). For Cs_2NaGaF_6, $t = 1.052$, and the observed $R\bar{3}m$ structure is predicted. On that basis, these facts become more consistent with Cr^{3+} occupation in Ga^{3+} rather than Na^{+} sites. The minor structural distortion of the $[GaF_6]$ octahedra caused by the Cr-ion impurity in Cs_2NaGaF_6, as shown in the x-ray data,

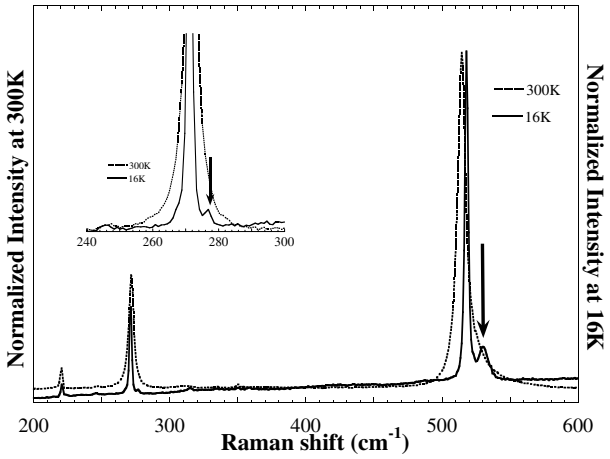

Figure 3. Evolution as a function of temperature (300 K: dotted curve; 16 K: full curve) of the Raman spectra for the polarization $Z(YY)Z$. As discussed in the text, the inclusion of Cr^{3+} into the Cs_2NaGaF_6 is confirmed by the 16 K Raman data, where the sidebands (at about 278 and 530 cm^{-1}, and indicated by arrows) are measurable. The inset shows in more detail the sideband located at 278 cm^{-1}. The slight increase of the background can be associated with luminescence effects.

is consistent with the close values calculated for the crystal-field parameters for both Cr^{3+} sites [17], $Dq/B \approx 2.2$. Moreover, the inclusion of Cr^{3+} into the Cs_2NaGaF_6 was confirmed by the 16 K Raman data, where the sidebands (at about 278 and 530 cm^{-1}) can be associated with the $\nu_{A_{1g}}$ modes arising from the formation of $[CrF_6]$ coordination units.

Now we turn to the discussion of the room temperature luminescence quantum yield (η) in the doped Cr^{3+} elpasolite lattices. Previous studies on Cr^{3+}-doped elpasolite systems have clearly demonstrated that lattice distortions and el–ph coupling are relevant to the multiphonon relaxation processes, and consequently the value of η for the system [5, 16]. In the particular case of Cs_2NaGaF_6:0.5Cr^{3+}, unlike Cs_2NaAlF_6:0.5% Cr^{3+} and other luminescent materials [8, 18], the vibrational properties of the $[CrF_6]^{3-}$ differ noticeably from those of the host lattice, and the large shift of 16 cm^{-1} between the bulk and the local mode frequency accounts for a strong el–ph coupling. This is indeed predictable given that gallium compounds, in general, present a high degree of covalence [19]. Consequently, in Cs_2NaGaF_6:Cr^{3+} we will observe an increase in the number of relaxation pathways [7], and a lower Cr^{3+} quantum yield should be observed compared to Cs_2NaAlF_6:Cr^{3+}, i.e. $\eta_{Cs_2NaAlF_6:Cr^{3+}} > \eta_{Cs_2NaGaF_6:Cr^{3+}}$. This assumption is further confirmed by structural arguments [20]. Considering that the smaller the host ion, the easier it is for the CrF_6^- unit to expand upon photon excitation, the displacement of the $^4T_2$ excited state [5] is smaller and more competitive with the radiative emission than the multiphonon relaxation. Therefore the room temperature quantum yield in the doped Cr^{3+} elpasolite lattices should follow the trend

$$\eta_{Cs_2NaAlF_6:Cr^{3+}}(r_{Al^{3+}} = 0.53) > \eta_{Cs_2NaGaF_6:Cr^{3+}}(r_{Ga^{3+}} = 0.62) > \eta_{Cs_2NaYBr_6:Cr^{3+}}(r_{Y^{3+}} = 0.9),$$

exactly as observed experimentally [18, 21, 22]. A value of η of about 0.3 and 0.4 was obtained, respectively, for Cs_2NaGaF_6:Cr^{3+} and Cs_2NaAlF_6:Cr^{3+}, while for Cs_2NaYBr_6:Cr^{3+}, η is about[5] 0.15.

[5] These values were calculated considering that a room temperature luminescence quantum yield of 100% is reached at 4.2 K.

In summary, the delicate balance between lattice and charge degrees of freedom observed in the Cr-doped halide elpasolite makes this system an excellent model for use to achieve a better understanding of multiphonon relaxation processes and thus also to explore the laser potential of new systems. We are currently investigating the laser potential of $Cs_2NaScF_6:Cr^{3+}$.

Acknowledgments

The authors wish to thank N M Khaidukov for providing the single-crystal materials for the optical studies, and D N Argyriou for helpful discussions. This work was supported by the UCSB-LANL (GRANT STB-UC:97-234) (HNB and GFS), DOE-BES under contract No W-31-109-Eng-38 (HNB and XW), and by FAPERJ, FINEP and CNPq (LPS, RJMF and ADT).

References

[1] Henderson B and Imbusch G F 1989 *Optical Spectroscopy of Inorganic Solids* (Oxford: Clarendon) and references therein
[2] Maiman T H 1960 *Nature* **187** 493
[3] Hammerling P, Budgor A B and Pinto A (ed) 1985 *Tunable Solid-State Lasers (Springer Series in Optical Science vol 47)* (Berlin: Springer)
[4] 1985 *Tunable Solid-State Lasers II (Springer Series in Optical Science vol 52)* (Berlin: Springer)
[5] Wenger O S and Güdel H U 2001 *J. Chem. Phys.* **114** 5832
[6] Wein G R, Hamilton D S, Sliwczuk U, Rinzler A G and Bartram R H 2001 *J. Phys.: Condens. Matter* **13** 2363
[7] da Fonseca R J M, Sosman L P, Dias Tavares A Jr and Bordallo H N 2000 *J. Fluoresc.* **10** 375
[8] Bordallo H N, Henning R W, Sosman L P, da Fonseca R J M, Tavares A D Jr, Hanif K M and Strouse G F 2001 *J. Chem. Phys.* **115** 4300
[9] Babel D and Haegele R 1976 *J. Solid State Chem.* **18** 39
[10] Hoppe R and Wingefeld G 1984 *Z. Anorg. Allg. Chem.* **519** 195
[11] Fargin E, Lestienne B and Dance J M 1990 *Solid State Commun.* **75** 769
[12] Villacampa B, Cases R and Alcala R 1995 *J. Lumin.* **63** 289
[13] Nakamoto K 1978 *Infrared and Raman Spectra of Inorganic and Coordination Compounds* (New York: Wiley)
[14] Tanner P A, Yulong L, Edelstein N M, Murdoch K M and Khaidukov N M 1997 *J. Phys.: Condens. Matter* **9** 7817
[15] Bartram R H, Wein G R and Hamilton D S 2001 *J. Phys.: Condens. Matter* **13** 2377
[16] Hehlen M P, Kuditcher A, Rand S and Tischler M 1997 *J. Chem. Phys.* **107** 4886
[17] da Fonseca R J M, Dias Tavares A Jr, Silva P S, Abritta T and Khaidukov N M 1999 *Solid State Commun.* **110** 519
[18] Blasse G and Dirksen G J 1992 *J. Solid State Chem.* **96** 258
[19] Vink A P and Meijerink A 2000 *J. Lumin.* **87–89** 601
[20] Blasse G and Bril A 1970 *Philips Tech. Rev.* **10** 31
[21] Sosman L P, Tavares A D Jr, da Fonseca R J M, Abritta T and Khaidukov N M 2000 *Solid State Commun.* **111** 661
[22] Knochenmuss R, Reber C, Rajasekharan M V and Güdel H U 1996 *J. Chem. Phys.* **85** 42802